9-2000

Mutations in the Hinge of a Dynamic Loop Broadly Influence Functional Properties of Fructose-1,6-bisphosphatase

Scott W. Nelson
Iowa State University, swn@iastate.edu

Jun-yong Choe
Iowa State University

Richard B. Honzatko
Iowa State University, honzatko@iastate.edu

Herbert J. Fromm
Iowa State University

Mutations in the Hinge of a Dynamic Loop Broadly Influence Functional Properties of Fructose-1,6-bisphosphatase

Abstract
Loop 52–72 of porcine fructose-1,6-bisphosphatase may play a central role in the mechanism of catalysis and allosteric inhibition by AMP. The loop pivots between different conformational states about a hinge located at residues 50 and 51. The insertion of proline separately at positions 50 and 51 reduces k_{cat} by up to 3-fold, with no effect on the K_m for fructose 1,6-bisphosphate. TheK_a for Mg^{2+} in the Lys^{50}→ Pro mutant increases ~15-fold, whereas that for the Ala^{51} → Pro mutant is unchanged. Although these mutants retain wild-type binding affinity for AMP and the fluorescent AMP analog 2′(3′)-*O*-(trinitrophenyl)adenosine 5′-monophosphate, the K_i for AMP increases 8000- and 280-fold in the position 50 and 51 mutants, respectively. In fact, the mutation Lys^{50} → Pro changes the mechanism of AMP inhibition with respect to Mg^{2+} from competitive to noncompetitive and abolishes K^+ activation. The K_i for fructose 2,6-bisphosphate increases ~20- and 30-fold in the Lys^{50} → Pro and Ala^{51} → Pro mutants, respectively. Fluorescence from a tryptophan introduced by the mutation of Tyr^{57}suggests an altered conformational state for Loop 52–72 due to the proline at position 50. Evidently, the Pro^{50} mutant binds AMP with high affinity at the allosteric site, but the mechanism of allosteric regulation of catalysis has been disabled.

Keywords
fructose bisphosphatase, enzyme activity, Adenosine Monophosphate, Alanine, Kinetics

Disciplines
Biochemistry | Chemistry | Molecular Biology

Comments
This article is from *Journal of Biological Chemistry* 275 (2000): 29986, doi: 10.1074/jbc.M000473200. Posted with permission.

THE JOURNAL OF BIOLOGICAL CHEMISTRY
Vol. 275, No. 39, Issue of September 29, pp. 29986–29992, 2000

Printed in U.S.A.

Mutations in the Hinge of a Dynamic Loop Broadly Influence Functional Properties of Fructose-1,6-bisphosphatase*

Received for publication, January 21, 2000, and in revised form, July 12, 2000
Published, JBC Papers in Press, July 14, 2000, DOI 10.1074/jbc.M000473200

Scott W. Nelson, Jun-Yong Choe, Richard B. Honzatko, and Herbert J. Fromm‡

From the Department of Biochemistry, Biophysics, and Molecular Biology, Iowa State University, Ames, Iowa 50011

Loop 52–72 of porcine fructose-1,6-bisphosphatase may play a central role in the mechanism of catalysis and allosteric inhibition by AMP. The loop pivots between different conformational states about a hinge located at residues 50 and 51. The insertion of proline separately at positions 50 and 51 reduces k_{cat} by up to 3-fold, with no effect on the K_m for fructose 1,6-bisphosphate. The K_a for Mg^{2+} in the $Lys^{50} \rightarrow Pro$ mutant increases ~15-fold, whereas that for the $Ala^{51} \rightarrow Pro$ mutant is unchanged. Although these mutants retain wild-type binding affinity for AMP and the fluorescent AMP analog 2′(3′)-*O*-(trinitrophenyl)adenosine 5′-monophosphate, the K_i for AMP increases 8000- and 280-fold in the position 50 and 51 mutants, respectively. In fact, the mutation $Lys^{50} \rightarrow Pro$ changes the mechanism of AMP inhibition with respect to Mg^{2+} from competitive to noncompetitive and abolishes K^+ activation. The K_i for fructose 2,6-bisphosphate increases ~20- and 30-fold in the $Lys^{50} \rightarrow Pro$ and $Ala^{51} \rightarrow Pro$ mutants, respectively. Fluorescence from a tryptophan introduced by the mutation of Tyr^{57} suggests an altered conformational state for Loop 52–72 due to the proline at position 50. Evidently, the Pro^{50} mutant binds AMP with high affinity at the allosteric site, but the mechanism of allosteric regulation of catalysis has been disabled.

Fructose-1,6-bisphosphatase (D-fructose-1,6-bisphosphate 1-phosphohydrase, EC 3.1.3.11; FBPase)[1] catalyzes the hydrolysis of fructose 1,6-bisphosphate (Fru-1,6-P_2) to Fru-6-P and P_i (for a review, see Refs. 1–3). FBPase is a tetramer of identical subunits (M_r = 37,000). Each subunit has binding sites for Fru-1,6-P_2, Fru-2,6-P_2, and metal ions (which, taken together, define the active site) and a distinct AMP-binding site (4–6). The two binding loci within the same subunit are 28 Å apart, lying for the most part in separate folding domains (called the AMP and Fru-1,6-P_2 domains). The four subunits of the tetramer occupy the corners of a rectangle, labeled clockwise C1 through C4, starting with the upper left-hand corner (7). FBPase exists in at least two conformational states, called R and T, which differ by a 17° rotation of the C1-C2 subunit pair with respect to the C3-C4 subunit pair about one of three intersecting 2-fold axes of the tetramer (7, 8).

Loop 52–72 could play an important role in the allosteric mechanism of AMP inhibition, existing in at least two conformational states (9, 10). In the absence of AMP, the loop interacts with the active site (engaged loop conformation), positioning the side chain of an essential catalytic residue, Asp^{74} (9, 11). The binding of AMP to its allosteric pocket putatively displaces the loop from the active site and stabilizes the disengaged loop conformation (9, 10). Subunits with disengaged loops evidently have reduced affinity for essential metal ions and, as a consequence, may be impaired with respect to catalysis. Mutations of conserved residues in Loop 52–72 have significant effects on catalysis and allosteric inhibition of catalysis by AMP (11).

The metabolic flux through FBPase is sensitive to prevailing levels of AMP and Fru-2,6-P_2. AMP inhibits FBPase allosterically with a Hill coefficient of 2 (12, 13), whereas Fru-2,6-P_2 inhibits FBPase by direct ligation of the active site with a Hill coefficient of unity (1–3). Inhibition of FBPase by AMP is nonlinear and noncompetitive with respect to Fru-1,6-P_2, but nonlinear and competitive with respect to Mg^{2+} (6, 14). In contrast, inhibition of FBPase by Fru-2,6-P_2 is linear and competitive with respect to Fru-1,6-P_2 and noncompetitive with respect to Mg^{2+}. Due to the equilibrium reaction catalyzed by adenylate kinase, concentrations of AMP *in vivo* are nearly constant under normal physiological conditions, whereas the concentration of Fru-2,6-P_2 varies in response to extracellular regulators such as glucagon and epinephrine. Hence, Fru-2,6-P_2 is the probable dynamic regulator of FBPase *in vivo*, but AMP still plays a significant role. Fru-2,6-P_2 lowers the apparent inhibition constant for AMP at least 10-fold (15) by decreasing the k_{off} of AMP (16). Levels of AMP association with the allosteric sites of FBPase will then necessarily change in response to Fru-2,6-P_2 levels, even if the concentration of AMP *in vivo* is constant. AMP/Fru-2,6-P_2 synergism may arise from the ability of each ligand to stabilize a common thermodynamic state of FBPase (disengaged Loop 52–72) through different mechanisms (9).

For Loop 52–72 to move between its various states, significant conformational change must occur in hinge elements at residues 50 and 51 and residues 71 and 72. The combined mutation of lysines 71 and 72 to methionine dramatically increases the K_i for AMP, presumably due to the stabilization of the R-state over the T-state conformer of FBPase (11). If the loop-mediated mechanism of AMP inhibition is valid, mutations at the second hinge element must qualitatively cause a similar increase in the K_i for AMP, yet mutations of Lys^{50} to methionine (17) and glutamine and alanine (18) cause virtually no change in the K_i for AMP. What is clear from crystal structures, however, is a large difference in main chain angles (ϕ, φ) at position 50 in the R- and T-states of FBPase (7, 9, 10). Here we explore the consequence of mutations $Lys^{50} \rightarrow Pro$ and

* This work was supported in part by National Institutes of Health Research Grant NS 10546 and National Science Foundation Grant MCB-9603595. This is Journal Paper 18895 of the Iowa Agriculture and Home Economic Experiment Station, Ames, IA, Project 3191. The costs of publication of this article were defrayed in part by the payment of page charges. This article must therefore be hereby marked "*advertisement*" in accordance with 18 U.S.C. Section 1734 solely to indicate this fact.

‡ To whom correspondence should be addressed. Tel.: 515-294-4971; Fax: 515-294-0453; E-mail: HJFromm@IASTATE.edu.

[1] The abbreviations used are: FBPase, fructose-1,6-bisphosphatase; Fru-1,6-P_2, fructose 1,6-bisphosphate; Fru-2,6-P_2, fructose 2,6-bisphosphate; TNP-AMP, 2′(3′)-*O*-(trinitrophenyl)adenosine 5′-monophosphate.

$Ala^{51} \rightarrow Pro$, which directly influence the backbone conformation of residues 50 and 51. The mutations have little effect on the binding affinity of a fluorescent analog of AMP, but increase the kinetic K_i value for that analog by several orders of magnitude. The kinetic K_m value for Fru-1,6-P_2 is unchanged by the mutations, but the K_a for Mg^{2+} rises 15-fold in the case of the Pro^{50} mutant and is 40-fold less active under standard conditions of assay. The data suggest that Loop 52–72 is an essential element in the allosteric mechanism of FBPase.

EXPERIMENTAL PROCEDURES

Materials—Fru-1,6-P_2, Fru-2,6-P_2, $NADP^+$, AMP, ampicillin, and isopropyl-β-D-thiogalactopyranoside were purchased from Sigma. DNA-modifying and restriction enzymes, T4 polynucleotide kinase, and ligase were from Promega. Glucose-6-phosphate dehydrogenase and phosphoglucose isomerase came from Roche Molecular Biochemicals. Tryptone, yeast extract, and agar were from Difco. Other chemicals were of reagent grade or equivalent. *Escherichia coli* strains BMH71-18 mutS and XL1-Blue came from CLONTECH and Stratagene, respectively. FBPase-deficient strain DF657 came from the Genetic Stock Center at Yale University.

Mutagenesis of Wild-type FBPase—Mutations were accomplished by specific base changes in double-stranded plasmid using the Transformer™ site-directed mutagenesis kit (CLONTECH). The mutagenic primers for the $Lys^{50} \rightarrow Pro$, $Ala^{51} \rightarrow Pro$, and $Tyr^{57} \rightarrow Trp$ mutants were 5′-GTCCGC**CCG**GCGGGCATC-3′, 5′-CCGCAAG**CCG**GGCATCGC-3′, and 5′-CGCACCTC**TGG**GGAATTG3′, respectively (codons for mutation are in boldface and underlined). The selection primer 5′-CAGCCTCGC**CTCGAG**AACGCCA-3′ (the digestion site is in boldface and underlined) changed an original *Nru*I site on the plasmid into a *Xho*I site. The mutation and integrity of the gene were confirmed by sequencing the entire gene. The Iowa State University sequencing facility provided DNA sequences using the fluorescent dye dideoxy terminator method.

Expression and Purification of Wild-type and Mutant FBPases—Protein expression and purification were performed as described previously (11), but with minor alterations. After cell breakage, FBPase was enriched and concentrated by 70% ammonium sulfate fractionation. The precipitate was taken up in 20 mM Tris (pH 7.5) and desalted on a Sephadex G-100 column using 20 mM Tris (pH 7.5). The active fractions were loaded directly onto a Cibacron blue column and eluted with a 0.5–1 M NaCl gradient. FBPase eluted at ~800 mM NaCl. The eluent was dialyzed against 20 mM Tris-HCl (pH 8.3), loaded onto a DEAE-Sephadex column, and then developed with a 0–300 mM NaCl gradient. FBPase eluted at a salt concentration of 150 mM, and its purity was confirmed by SDS-polyacrylamide gel electrophoresis (19). Protein concentration was determined using the Bradford assay (20) with bovine serum albumin as a standard.

Circular Dichroism Spectroscopy—CD studies on wild-type and mutant FBPases were done at room temperature on a Jasco J710 CD spectrometer in a 1-cm cell using a protein concentration of 0.35 mg/ml. Spectra were collected from 200 to 260 nm in increments of 1.3 nm. Each spectrum was blank-corrected and smoothed using the software package provided with the instrument.

Kinetic Experiments—Assays for the determination of specific activity, k_{cat}, and activity ratios at pH 7.5 and 9.5 employed the coupling enzymes phosphoglucose isomerase and glucose-6-phosphate dehydrogenase (1). The reduction of $NADP^+$ to NADPH was monitored directly at 340 nm. All other assays employed the same coupling enzymes, but monitored NADPH evolution by its fluorescence emission at 470 nm (excitation wavelength of 340 nm). Initial rate data were analyzed using either programs written in the MINITAB language using an α value of 2.0 (14) or ENZFITTER (21). The kinetic data were fit to a variety of models. Only models and parameters for the best fits are reported below.

Steady-state Fluorescence Measurements—Fluorescence data were collected using an SLM 8100C fluorometer (Spectronic Instruments). The single tryptophan in the Trp^{57} mutant was excited selectively using radiation of 295-nm wavelength. Fluorescence emission spectra were recorded in steps of 1 nm from 310 to 400 nm using a slit width of 2 mm for both excitation and emission. Each spectrum was an average of five scans. Fluorescence from TNP-AMP employed excitation and emission wavelengths of 400 and 535 nm, respectively. Conditions under which specific spectra were recorded are provided below and in the tables and figure legends. Each point is the average of 15 1-s acquisitions. Enzyme concentrations ranged from 0.3 to 0.5 μM. All spectra were corrected for dilution and inner filter effects (absorbance of light by AMP and TNP-AMP) using Equation 1 (22),

$$F_c = (F - B)(V_i/V_0)10^{(A_{ex}+A_{em})/2} \quad \text{(Eq. 1)}$$

where F_c is the corrected fluorescence, F is the fluorescence intensity experimentally measured, B is the background, V_i is the volume of the sample for a specific titration point, V_0 is the initial volume of the sample, A_{ex} is the absorbance measured at the wavelength of excitation (295 nm for AMP and 410 nm for TNP-AMP), and A_{em} is the absorbance measured at the wavelength of emission (535 nm for TNP-AMP). As a control, ligands by themselves caused no change in fluorescence emission from a solution of tryptophan (100 μM).

TNP-AMP titration data were analyzed by nonlinear least-squares fits using Equation 2,

$$\frac{\Delta F}{F_o} = \frac{(\Delta F_{max}/F_0) \cdot L^n}{K_d + L^n} \quad \text{(Eq. 2)}$$

where ΔF is the change in fluorescence caused by the addition of ligand (L), F_0 is the fluorescence in the absence of ligand, ΔF_{max} is the theoretical maximum change in fluorescence at saturating ligand concentration, K_d is the dissociation constant, and n is the Hill coefficient.

Structural Modeling of FBPase Mutants—The starting model for the engaged conformation of Loop 52–72 is the crystal structure of the Zn^{2+}·product complex of FBPase (PDB accession code 1CNQ), in which the tetramer assumes the R-state conformation (9). The starting model for the disengaged conformation of Loop 52–72 is a Zn^{2+}·product·AMP complex of FBPase, in which the tetramer has the T-state conformation (10). The latter structure is similar to other T-state structures of FBPase (7, 23), differing primarily in the ligands present at the active site. Proline residues were placed individually at positions 50 and 51 using the software XTALVIEW and a Silicon Graphics workstation. The initial models were passed through three protocols: 1) 100 cycles of conjugate gradient minimization; 2) 100 cycles of conjugate gradient minimization, followed by simulated annealing (starting temperature, 500 K; final temperature, 300 K) (24) and then another 100 cycles of conjugate gradient minimization; and 3) the same procedure as Protocol 2, but using a starting temperature of 1000 K. During simulated annealing and energy minimization, the C^α atoms (except for residues 50–72) were restrained to their initial crystallographic positions by a harmonic pseudo-potential with a force constant of 50 kcal/mol. The justification for restraining all C^α atoms outside of the loop is the 10-year history of FBPase crystal structures, which collectively reveal only small changes in the protein conformation outside of Loop 52–72.

RESULTS

Modeling of FBPase Mutants—A structural overview of the region of interest is provided in Fig. 1. The main chain ϕ angle of Lys^{50} differs significantly in the T- and R-states, neither value being compatible with that of proline, where ϕ must be close to −60°. Insertion of proline then results in an initial model with poor stereochemistry at position 50. Energy minimization alone and energy minimization with simulated annealing at a starting temperature of 500 K (Protocols 1 and 2 in "Experimental Procedures") leave the ϕ angle of Pro^{50} some 30° away from its preferred value in both the T- and R-states. Further improvement in the stereochemistry of Pro^{50} requires a starting temperature of 1000 K in simulated annealing (Protocol 3), the consequence of which is a significant drift of the Loop 52–72 away from either its T- or R-state conformation. Evidently, proline at position 50 is incompatible with the T-state disengaged and R-state engaged loop conformations.

Proline at position 51, on the other hand, is less disruptive. The ϕ angle of residue 51 is near −60° in both the R- and T-states of FBPase. Backbone amide 51 hydrogen bonds with backbone carbonyls 47 and 48 in the R-state and with backbone carbonyl 46 in the T-state. Proline substitution at position 51 clearly disrupts the hydrogen bonds in both the R- and T-states. Moreover, the C^δ atom of proline makes close contacts of 1.9 and 1.8 Å with backbone carbonyls 48 (R-state) and 46 (T-state), respectively. Either energy minimization alone or energy minimization with simulated annealing (initial temperature, 500 K) relaxes the contact in the R-state (the loop re-

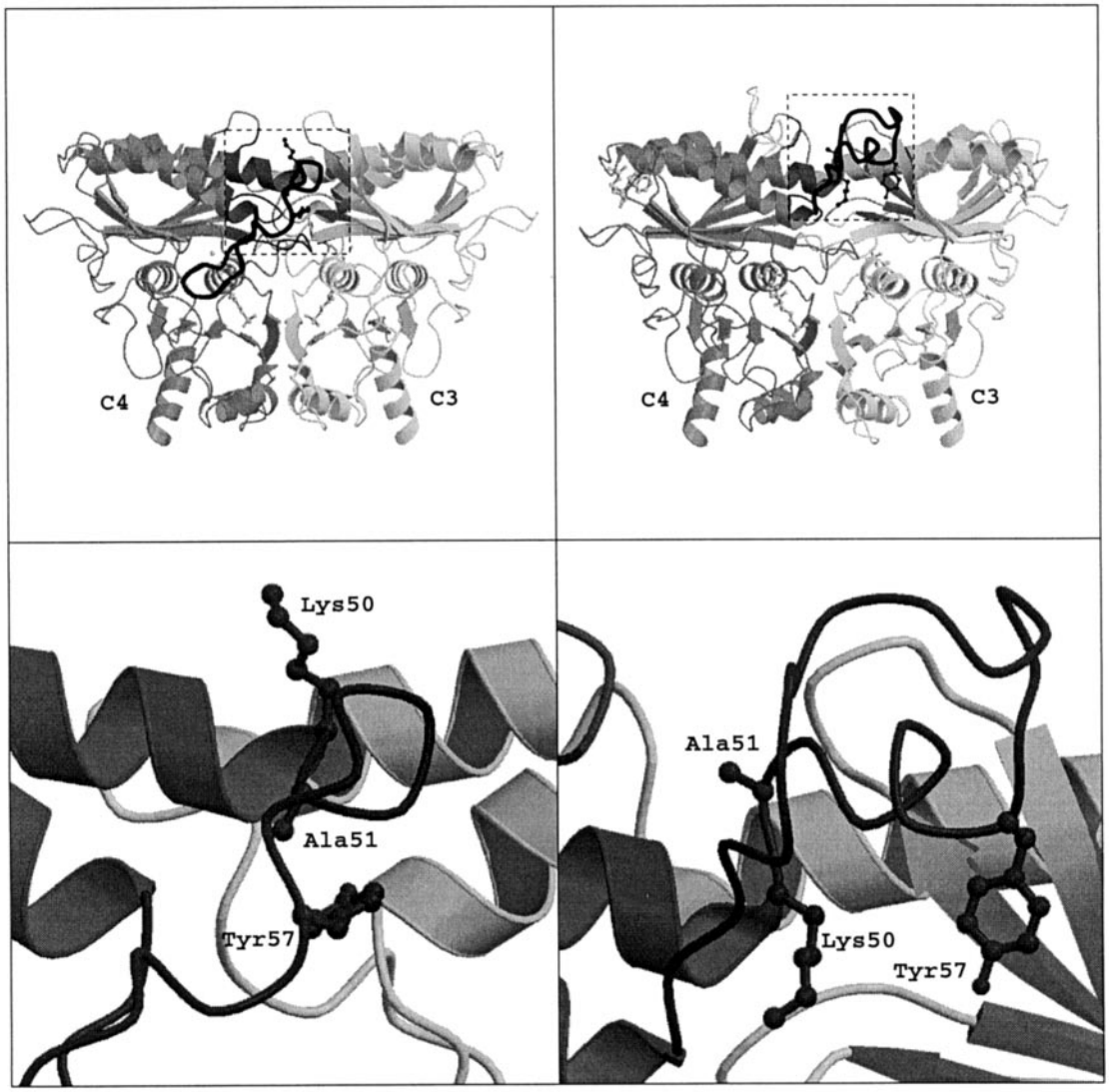

FIG. 1. **Wild-type FBPase in the T- and R-states.** The *upper panels* show only the C3-C4 subunit pair from the R-state (*left panel*) and T-state (*right panel*) tetramers. Loop 52–72 from subunit C4 is represented by a *thick black line*. The regions within the *dashed boxes* are enlarged in the *lower panels*, showing the relative positions of Lys^{50}, Ala^{51}, and Tyr^{57}. This figure was prepared with MOLSCRIPT (32) and RASTER3D (33).

mains engaged with the active site) by a 90° rotation of the plane of the polypeptide linkage between residues 47 and 48. The close contact of the T-state remains, however, at 2.4 and 2.8 Å after modeling Protocols 1 and 2, respectively. Contacts from within the subunit and from the neighboring subunit constrain the T-state conformation of residues 52–57 (Fig. 1). Furthermore, as backbone carbonyl 46 is an integral part of helix H2, it cannot relieve its close contact with Pro^{51} by a rotation of its polypeptide linkage. Hence, proline at position 51 probably increases the internal energy of the T-state, destabilizing it relative to the R-state of FBPase.

Expression and Purification of Wild-type and Mutant FBPases—Mutant and wild-type FBPases behaved identically throughout purification, including gel exclusion chromatography. The wild-type and mutant enzymes were at least 95% pure with no evidence for proteolysis on the basis of SDS-polyacrylamide gel electrophoresis.

Secondary Structure Analysis—The CD spectra of wild-type FBPase in the T- and R-states diverge minimally, but reproducibly in the vicinity of 210 nm (17). The CD spectra of the $Ala^{51} \rightarrow Pro$, $Lys^{50} \rightarrow Pro/Tyr^{57} \rightarrow Trp$, and wild-type FBPases superimpose in the presence of P_i (5 mM), Fru-6-P (5 mM), and saturating Mg^{2+} (5 mM for the wild-type and $Ala^{51} \rightarrow Pro$ enzymes and 35 mM for $Lys^{50} \rightarrow Pro/Tyr^{57} \rightarrow Trp$). The addition of AMP (200 μM) to the wild-type enzyme produced small changes in the CD spectrum near 210 nm, as noted above, but caused no change in the CD spectra of the $Lys^{50} \rightarrow Pro/Tyr^{57} \rightarrow Trp$ and $Ala^{51} \rightarrow Pro$ enzymes. (Concentrations of AMP in excess of 200 μM degraded CD spectra due to the elevated absorbance of radiation.) The CD spectra of the $Lys^{50} \rightarrow Pro$ mutant also differ from the corresponding wild-type spectra (Fig. 2). The CD spectrum of the $Lys^{50} \rightarrow Pro$ mutant did not change in the presence of P_i (5 mM), Fru-6-P (5 mM), and saturating Mg^{2+} (50 mM) in the presence or absence of AMP (200 μM).

Catalytic Rates, Michaelis Constants for Mg^{2+} and Fru-1,6-P_2, and K^+ Activation—Initial rate kinetics employ maximal substrate concentrations, sufficient to saturate the active site, but low enough to avoid substrate inhibition. The ratios of catalytic rate constants at pH 7.5 and 9.6 are comparable for wild-type and $Ala^{51} \rightarrow Pro$ FBPases (Table I), both consistent with reported activity ratios for an FBPase free of proteolysis. The activity ratios for the $Lys^{50} \rightarrow Pro$ and $Lys^{50} \rightarrow Pro/Tyr^{57} \rightarrow Trp$ mutants are low, however; but as discussed below, the low value does not stem from limited proteolysis of that mutant.

All enzymes have comparable K_m values for Fru-1,6-P_2 (Table I); but beyond this, the quantitative similarities end. Under standard conditions of assay for the wild-type enzyme (5 mM Mg^{2+} and 20 μM Fru-1,6-P_2, pH 7.5), the mutation of Lys^{50} to proline resulted in a 40-fold loss of specific activity. However, the decline in specific activity was due primarily to a 15-fold increase in the K_a for Mg^{2+} for the Pro^{50} mutant. The k_{cat} value for the Pro^{50} mutant (saturated with Mg^{2+}) is one-third of that for the wild-type enzyme. The Hill coefficients for Mg^{2+} for the $Ala^{51} \rightarrow$ Pro, $Lys^{50} \rightarrow$ Pro/$Tyr^{57} \rightarrow$ Trp, and wild-type enzymes are similar, but are reduced significantly in the $Lys^{50} \rightarrow$ Pro mutant. Potassium ion activation is retained in the $Ala^{51} \rightarrow$ Pro and $Lys^{50} \rightarrow$ Pro/$Tyr^{57} \rightarrow$ Trp mutants at levels comparable to that of the wild-type enzyme, but is abolished altogether in the Pro^{50} mutant.

Kinetics of AMP Inhibition—Concentrations of AMP needed for 50% inhibition increased 280-, 8000-, and 400-fold relative to that of the wild-type enzyme for the $Ala^{51} \rightarrow$ Pro, $Lys^{50} \rightarrow$ Pro, and $Lys^{50} \rightarrow$ Pro/$Tyr^{57} \rightarrow$ Trp mutants, respectively (Fig. 3 and Table I). Additionally, the $Lys^{50} \rightarrow$ Pro/$Tyr^{57} \rightarrow$ Trp double mutant displays biphasic behavior toward AMP. The data of Fig. 3 for the wild-type, $Ala^{51} \rightarrow$ Pro, and $Lys^{50} \rightarrow$ Pro enzymes were fit to Equation 3,

$$v = \frac{V_0}{\left(1 + \left(\frac{I}{IC_{50}}\right)^2\right)} \qquad \text{(Eq. 3)}$$

where v is the observed velocity at a specific concentration of AMP, V_0 is the fitted velocity in the absence of AMP, I is the concentration of AMP, and IC_{50} is the concentration of AMP that causes 50% inhibition. The exponent of 2 represents the Hill coefficient for AMP cooperativity, determined independently as described below. The data of Fig. 3 for $Lys^{50} \rightarrow$ Pro/$Tyr^{57} \rightarrow$ Trp FBPase were fit to Equation 4,

$$v = \frac{V_0}{\left(1 + \left(\frac{I}{IC_{50\text{-high}}}\right)^2 + \left(\frac{I}{IC_{50\text{-low}}}\right)^n\right)} \qquad \text{(Eq. 4)}$$

where v, V_0, and I are as defined above for Equation 3 and $IC_{50\text{-high}}$ and $IC_{50\text{-low}}$ represent concentrations of AMP that cause 50% relative inhibition due to the ligation of high and low affinity sites, respectively. Ligation of the high affinity sites, as shown below, is cooperative with a Hill coefficient of 2, whereas the cooperativity with respect to the ligation of low affinity sites is an adjustable parameter (n) in Equation 4. The fitted value for n is 1.4.

AMP inhibition of wild-type FBPase is nonlinear and noncompetitive with respect to Fru-1,6-P_2 and nonlinear and competitive with respect to Mg^{2+}. The $Ala^{51} \rightarrow$ Pro mutant retains the nonlinear, competitive relationship between AMP and Mg^{2+} (goodness-of-fit, 5.5%) (Fig. 4), consistent with Equation 5,

$$\frac{1}{v} = \frac{1}{V_m}\left(1 + \frac{K_a}{A^2}\left(1 + \frac{I^n}{K_i}\right)\right) \qquad \text{(Eq. 5)}$$

where v, V_m, A, I, K_a, K_i, and n represent initial velocity, maximal velocity, Mg^{2+} concentration, AMP concentration, the Michaelis constant for Mg^{2+}, the dissociation constant for AMP from the enzyme·AMP complex, and the Hill coefficient for AMP, respectively. The binding of AMP is cooperative at $n = 2$, whereas cooperativity is absent when $n = 1$. Data from the wild-type and $Ala^{51} \rightarrow$ Pro enzymes are consistent with $n = 2$ (AMP cooperativity). When assayed at low AMP concentrations, $Lys^{50} \rightarrow$ Pro/$Tyr^{57} \rightarrow$ Trp retains the competitive mech-

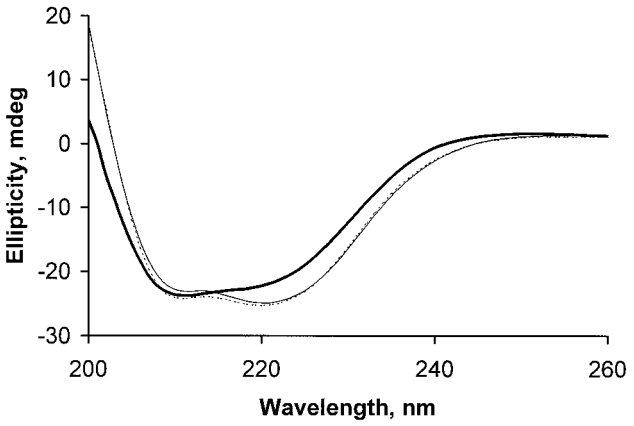

FIG. 2. **CD spectra for wild-type and $Lys^{50} \rightarrow$ Pro FBPases.** *Thin solid line*, R-state wild-type enzyme with reaction products and Mg^{2+}; *dotted line*, T-state wild-type enzyme with reaction products, Mg^{2+}, and AMP; *thick solid line*, $Lys^{50} \rightarrow$ Pro mutant under either R- or T-state conditions. *mdeg*, millidegrees.

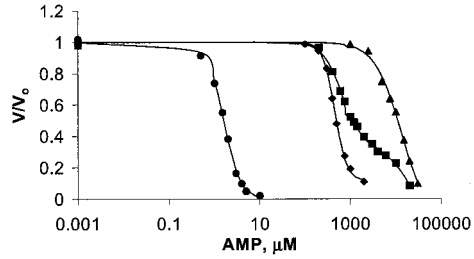

FIG. 3. **AMP inhibition of wild-type and mutant FBPases.** AMP titrations were of wild-type (●), $Ala^{51} \rightarrow$ Pro (♦), $Lys^{50} \rightarrow$ Pro/$Tyr^{57} \rightarrow$ Trp (■), and $Lys^{50} \rightarrow$ Pro (▲) FBPases in saturating Fru-1,6-P_2 (20 μM) and a Mg^{2+} concentration equal to the K_a for Mg^{2+} of each enzyme. See "Results" for details regarding the fitted curves.

TABLE I
Kinetic parameters for wild-type and mutant forms of fructose-1,6-bisphosphatase

	7.5/9.5 ratio	Specific activity[a]	k_{cat} [b]	K_m for Fru-1,6-P_2	K_a for Mg^{2+}	Hill for Mg^{2+}	K_i for Fru-2,6-P_2	IC_{50} for AMP[c]	K^+activation[d]
		units/mg/s	s^{-1}	μM	mM^2		μM	μM	%
Wild-type	3.3	35 ± 2	22 ± 1	1.75 ± 0.09	0.67 ± 0.04	1.9 ± 0.1	0.123 ± 0.005	1.61 ± 0.05	16.8 ± 0.3
$Lys^{50} \rightarrow$ Pro	0.93	0.85 ± 0.06	6.7 ± 0.3	2.1 ± 0.2	10.7 ± 0.8	1.45 ± 0.08	2.3 ± 0.2	13400 ± 20	−4.32 ± 0.04
$Ala^{51} \rightarrow$ Pro	3.2	20 ± 1	12.4 ± 0.7	2.5 ± 0.2	0.8 ± 0.1	2.1 ± 0.2	3.4 ± 0.2	460 ± 7	15.9 ± 0.1
$Tyr^{57} \rightarrow Trp$[e]	3.3	38.6 ± 0.1	24.0 ± 0.1	3.39 ± 0.09	0.53 ± 0.06	1.9 ± 0.1	0.84 ± 0.05	8.5 ± 0.4	16.6 ± 0.4
$Lys^{50} \rightarrow$ Pro/ $Tyr^{57} \rightarrow$ Trp	1.9	8.7 ± 0.8	9.2 ± 0.5	1.3 ± 0.1	3.1 ± 0.2	1.80 ± 0.07	0.37 ± 0.03	650 ± 40[f]	14.6 ± 0.1

[a] Specific activity was determined at 5 mM Mg^{2+} and 20 μM Fru-1,6-P_2.
[b] k_{cat} is defined as V_{max}/E_T, where E_T is the total enzyme concentration.
[c] The Hill coefficient for AMP ligation of high affinity sites is 2. See "Results" for details.
[d] K^+ activation is the percent increase in V_{max} using 150 mM KCl *versus* 0 mM KCl at saturating Mg^{2+} and Fru-1,6-P_2.
[e] Data are from Ref. 25.
[f] The reported value is for the high affinity site ($IC_{50\text{-high}}$). $IC_{50\text{-low}}$ is 28 ± 6 mM with a Hill coefficient of 1.4. See "Results" for details.

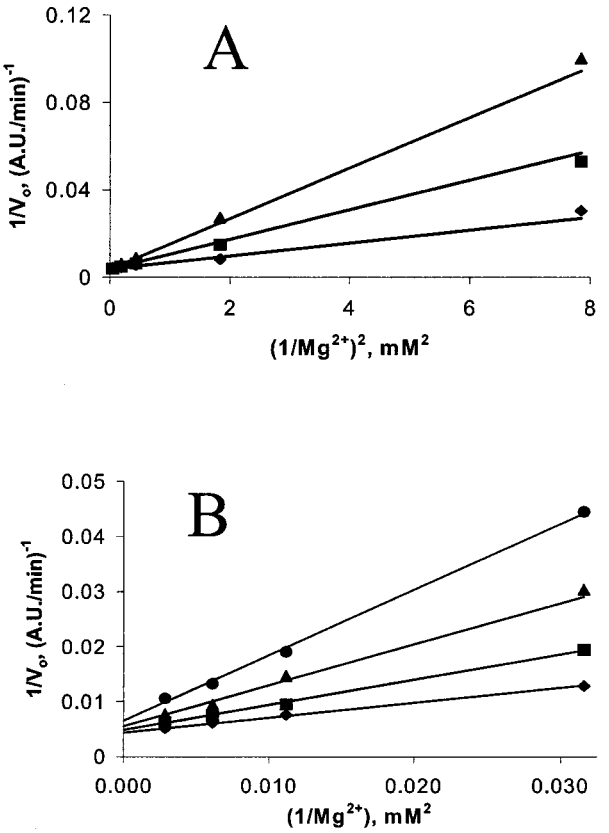

FIG. 4. **Kinetic mechanism of inhibition of Ala^{51} → Pro and Lys^{50} → Pro FBPases.** *A*, AMP competes with Mg^{2+} in the Ala^{51} → Pro mutant. Concentrations of AMP were 0 (♦), 100 μM (■), and 225 μM (▲). *B*, AMP inhibition is noncompetitive with respect to Mg^{2+} in the Lys^{50} → Pro mutant. Concentrations of AMP were 0 (♦), 10 mM (■), 15 mM (▲), and 20 mM (●). All assays were performed at saturating concentrations of Fru-1,6-P_2 (20 μM) and at 150 mM KCl. The lines are based upon Equation 5 for *A* and Equation 6 for *B* using the parameters of Table I. *A.U.*, arbitrary units.

anism with $n = 2$. In contrast, AMP inhibition of the Lys^{50} → Pro mutant fits best to a mechanism of noncompetitive inhibition with respect to Mg^{2+} (goodness-of-fit, 3.1%) (Fig. 4), represented by Equation 6,

$$\frac{1}{v} = \frac{1}{V_m}\left(1 + \frac{1^n}{K_{ii}} + \frac{K_a}{A}\left(1 + \frac{I^n}{K_i}\right)\right) \quad \text{(Eq. 6)}$$

where the terms of Equation 6 are defined as for Equation 5 and K_{ii} represents the dissociation constant for AMP from the enzyme·Mg^{2+}·AMP complex. The data are consistent with $n = 2$, reflecting AMP cooperativity.

In wild-type, Ala^{51} → Pro, and Lys^{50} → Pro/Tyr^{57} → Trp FBPases, the mechanism of AMP inhibition with respect to Fru-1,6-P_2 is nonlinear and noncompetitive (Equation 7),

$$\frac{1}{v} = \frac{1}{V_m}\left(1 + \frac{I^n}{K_{ii}} + \frac{K_b}{B}\left(1 + \frac{I^n}{K_i}\right)\right) \quad \text{(Eq. 7)}$$

where v, V_m, I, and n are as defined above, K_i and K_{ii} represent the dissociation constants for AMP from the enzyme·AMP and the enzyme·Fru-1,6-P_2·AMP complexes, respectively, B is the concentration of Fru-1,6-P_2, and K_b is the Michaelis constant for Fru-1,6-P_2. The high value for IC_{50} associated with AMP inhibition of the Lys^{50} → Pro mutant (Table I) precludes the determination of a kinetic mechanism.

Kinetics of Fru-2,6-P_2 Inhibition—Fru-2,6-P_2 is a competitive inhibitor with respect to Fru-1,6-P_2 for the position 50 and 51 mutant FBPases. The data best fit to Equation 8 (goodness-of-fit, 4.0%),

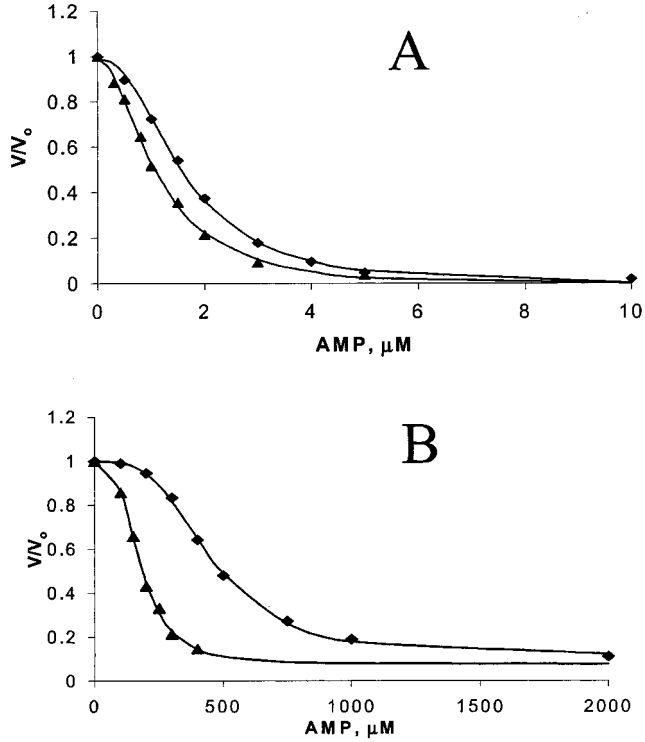

FIG. 5. **AMP/Fru-2,6-P_2 synergism for wild-type (*A*) and Ala^{51} → Pro (*B*) FBPases.** The concentrations of Fru-2,6-P_2 were 0 (♦) and approximately one-fourth of the K_i for Fru-2,6-P_2 (0.03 μM for wild-type FBPase and 0.86 μM for the Ala^{51} → Pro mutant) (▲). Assays had Mg^{2+} concentrations equal to the K_a for Mg^{2+} of each enzyme and saturating levels of Fru-1,6-P_2 (20 μM).

TABLE II
Inhibition and binding constants for TNP-AMP for wild-type and mutant forms of fructose-1,6-bisphosphatase

	IC_{50} for TNP-AMP	K_d for TNP-AMP
	μM	μM
Wild-type	7.4 ± 0.7	13.1 ± 0.6
Lys^{50} → Pro	ND[a]	14 ± 4
Ala^{51} → Pro	ND	37 ± 2

[a] Not determined due to weak inhibition by TNP-AMP.

$$\frac{1}{v} = \frac{1}{V_m}\left(1 + \frac{K_b}{B}\left(1 + \frac{I}{K_i}\right)\right) \quad \text{(Eq. 8)}$$

where v, V_m, I, B, K_i, and K_b are as defined above. The kinetic mechanism of Fru-2,6-P_2 inhibition is the same for mutant and wild-type FBPases, but the K_i for Fru-2,6-P_2 is ~20-, 30-, and 3-fold higher in the Lys^{50} → Pro, Ala^{51} → Pro, and Lys^{50} → Pro/Tyr^{57} → Trp mutants, respectively, relative to the wild-type enzyme (Table I).

Fru-2,6-P_2 and AMP Synergism—AMP and Fru-2,6-P_2 synergistically inhibited wild-type and mutant FBPases (Fig. 5). For all enzymes, the Hill coefficient for AMP is 2. At high concentrations of Fru-2,6-P_2, the saturation curve for Fru-1,6-P_2 changes from hyperbolic to sigmoidal for mutant and wild-type enzymes.

Steady-state Fluorescence Measurements—TNP-AMP inhibited the wild-type enzyme competitively with respect to Mg^{2+} and inhibited FBPase synergistically with Fru-2,6-P_2. Fluorescence emission from TNP-AMP increased significantly in the presence of FBPase. In addition, AMP reduced the fluorescence from bound TNP-AMP, presumably through competition for the allosteric effector site (data not shown). TNP-AMP bound to wild-type, Lys^{50} → Pro, and Ala^{51} → Pro FBPases with high

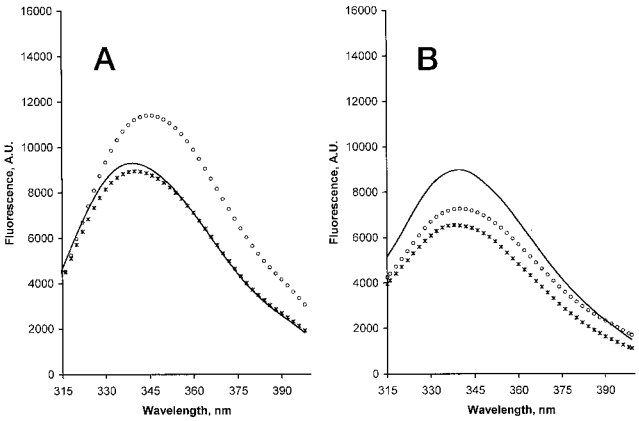

FIG. 6. **Fluorescence spectra of the Trp^{57} and Trp^{57}/Pro^{50} mutants.** In all cases, apoenzymes were in 50 mM Hepes (pH 7.5). Product complexes had 5 mM Fru-6-P and 5 mM potassium P_i with either 5 or 35 mM Mg^{2+} for the Trp^{57} and Trp^{57}/Pro^{50} mutants, respectively. *A*, Trp^{57} mutant. *Black line*, apoenzyme; *open circles*, product complex; *asterisks*, product complex + 400 μM AMP. *B*, Pro^{50}/Trp^{57} mutant. *Black line*, apoenzyme; *open circles*, product complex; *asterisks*, product complex + 20 mM AMP. *A.U.*, arbitrary units.

affinity, comparable to AMP. On the basis of fluorescence titration data (Table II), however, the Hill coefficient for TNP-AMP is near unity in all cases.

FBPase has no tryptophan, so the mutation of any single residue to tryptophan introduces a unique fluorophore. Fluorescence emission from tryptophan at position 57 is sensitive to the conformational state of Loop 52–72. The indole of Trp^{57} is exposed to solvent in the T-state disengaged loop conformation, whereas it resides in a hydrophobic pocket in the R-state engaged loop conformation. The $Tyr^{57} \rightarrow$ Trp mutant has been thoroughly studied by x-ray crystallography and initial velocity kinetics (25). Fluorescence emission spectra from the Pro^{50}/Trp^{57} double mutant differ significantly from those of the Trp^{57} single mutant (Fig. 6). Fluorescence emission from the single Trp^{57} mutant is maximum in the presence of products/metals, conditions that promote the R-state engaged loop conformation (9, 10). The addition of AMP reduced fluorescence emission to a level comparable to that observed from the Trp^{57} mutant in the absence of products and metals (apo form of FBPase). In contrast, the apo form of the Pro^{50}/Trp^{57} double mutant has the highest fluorescence emission. The addition of either product/metals or product/metals/AMP caused only a decrease in fluorescence emission.

DISCUSSION

Low activity ratios (~0.3) are a property of wild-type FBPase after limited proteolysis by papain or subtilisin (26). The maximum effect on the activity ratio due to proteolysis occurs when one subunit per tetramer is cut. Thus, for the wild-type enzyme, an activity ratio of 1, as observed for the $Lys^{50} \rightarrow$ Pro mutant, requires an equal mixture of intact and once-proteolyzed tetramers. Proteolysis of one of eight subunits then could account for a diminished activity ratio in any FBPase. In SDS-polyacrylamide gel electrophoresis of the $Lys^{50} \rightarrow$ Pro mutant, however, no fragments typical of proteolysis were evident. Furthermore, loss of AMP inhibition due to proteolysis of wild-type FBPase varied proportionately with the extent of subunit cleavage. The 8000-fold increase in K_i for AMP far exceeds the effect on AMP inhibition due to proteolysis, even in a completely proteolyzed system. Hence, the kinetic properties of the $Lys^{50} \rightarrow$ Pro mutant are not the consequence of proteolysis, but rather the influence of a proline at position 50.

Allosteric inhibition of wild-type FBPase by TNP-AMP is essentially identical to that caused by AMP, the only difference being the absence of cooperativity in the kinetics and in the binding of the fluorescent analog. In fact, TNP-AMP is indistinguishable from formycin 5′-monophosphate in its inhibition and binding to wild-type FBPase. Formycin 5′-monophosphate also exhibits a Hill coefficient of unity (27), and crystal structures of complexes of formycin 5′-monophosphate and AMP with human FBPase are identical (28). The difference in Hill coefficient may stem from subtle differences in conformation, evident perhaps only in partially ligated states of FBPase. Nonetheless, the fluorescence data clearly demonstrate tight binding of TNP-AMP and the displacement of that analog from FBPase by the addition of AMP. Hence, wild-type and Pro^{50} mutant FBPases are indistinguishable in their binding of TNP-AMP and its displacement by AMP.

On the basis of kinetics, however, Pro^{50} mutant FBPase is altogether insensitive to AMP. Inhibition of the Pro^{50} mutant by AMP requires an 8000-fold increase in ligand concentration and exhibits a different kinetic mechanism (noncompetitive *versus* competitive with respect to Mg^{2+}). The apparent change in kinetic mechanism may arise from the unmasking of a secondary mechanism, due to the complete loss of allosteric inhibition by AMP. That secondary mechanism may be the direct coordination of AMP to the metal-ligated active site of Pro^{50} mutant FBPase. Hence, if AMP binds tightly to the Pro^{50} mutant, as evidenced by the fluorescence data, but does not inhibit, then proline at position 50 must interrupt the transmission of the allosteric signal.

Kinetic data indicate the disruption of Loop 52–72 as the root cause for the loss of allosteric properties in Pro^{50} mutant FBPase. The K_a for Mg^{2+} is elevated 15-fold in the Pro^{50} mutant, and K^+ activation is lost. The kinetic mechanism of AMP inhibition with respect to Mg^{2+} is competitive in wild-type FBPase. Hence, in wild-type FBPase, AMP elevates the apparent dissociation constant of metals. A greatly elevated K_a for Mg^{2+}, accompanied by the complete loss of AMP inhibition, is consistent with an FBPase unable to achieve its high affinity state for metal cations. On the basis of recent crystal structures (10), the R-state engaged conformation of Loop 52–72 represents the high affinity state for metal cations and the catalytically productive state of FBPase. Pro^{50} mutant FBPase then cannot achieve a engaged loop conformation.

Molecular modeling, CD spectroscopy, and fluorescence emission from Trp^{57} strengthen the argument above. The mutation of Lys^{50} to proline destabilizes the R-state engaged loop and T-state disengaged loop conformations in slow cooling/energy minimization protocols. The CD spectrum of Pro^{50} mutant FBPase supports an altered state, conformationally unresponsive to the binding of ligands. The indole group of Trp^{57} in the Pro^{50}/Trp^{57} double mutant does not enter its hydrophobic pocket, as evidenced by the low fluorescence emission in the presence of saturating products/metals. The several lines of evidence provided here suggest that Loop 52–72 in Pro^{50} mutant FBPase can achieve neither its T-state disengaged nor its R-state engaged loop conformation. The complete loss of allosteric inhibition in Pro^{50} mutant FBPase suggests furthermore, that Loop 52–72 is an essential element in the allosteric regulation of FBPase.

The effects of the $Ala^{51} \rightarrow$ Pro mutation are less dramatic, in harmony with the results of modeling and CD spectroscopy. The Pro^{51} mutant retains K^+ activation and wild-type affinity for divalent cations, but exhibits a significant increase in the K_i for AMP. The mutation evidently destabilizes the T-state disengaged conformation of Loop 52–72 relative to the R-state engaged conformation, again consistent with the results of modeling. In this respect, the Pro^{51} mutant and the $Met^{71/72}$ double mutant (11) have similar effects on FBPase function. In

both instances, lessened AMP inhibition probably arises from a perturbation in the equilibrium between engaged and disengaged loop conformations in favor of the engaged state.

The K_i for Fru-2,6-P_2 increases 20- and 30-fold in the $Lys^{50} \rightarrow$ Pro and $Ala^{51} \rightarrow$ Pro mutants, respectively. The change in binding affinity for Fru-2,6-P_2 in these mutants must be indirect and is most likely through a perturbation of conformation states accessible to Loop 52–72. The increase in K_i for Fru-2,6-P_2 due to loop mutations does not come with an increase in the K_m for Fru-1,6-P_2, as has been observed in other mutations that increase the K_i for Fru-2,6-P_2 (29). The observation above is consistent with findings that suggest that Fru-2,6-P_2 and Fru-1,6-P_2, although binding at the same site, evoke different conformational responses from FBPase. For instance, at high concentrations of Fru-2,6-P_2, the Hill coefficient for AMP inhibition changes from 2 to 1, and the saturation curve for Fru-1,6-P_2 changes from hyperbolic to sigmoidal (3, 30). At low concentrations of Fru-2,6-P_2, the Hill coefficient for Mg^{2+} changes from 2 to 1 (31). Finally, Fru-2,6-P_2 protects FBPase from loss of AMP inhibition and catalytic activity due to modification by acetylimidazole, whereas Fru-1,6-P_2 protects only against loss of activity (31). Although a complete understanding of the above phenomena will come with further study, mutations of the loop underscore a fundamental difference in FBPase in its Fru-2,6-P_2- and Fru-1,6-P_2-ligated states.

Acknowledgment—We thank Xiaofeng Liu for technical assistance in the preparation of the Pro^{50} /Trp^{57} double mutant plasmid.

REFERENCES

1. Benkovic, S. T., and de Maine, M. M. (1982) *Adv. Enzymol. Relat. Areas Mol. Biol.* **53,** 45–82
2. Tejwani, G. A. (1983) *Adv. Enzymol. Relat. Areas Mol. Biol.* **54,** 121–194
3. Van Schaftingen, E. (1987) *Adv. Enzymol. Relat. Areas Mol. Biol.* **59,** 45–82
4. Ke, H., Zhang, Y., Liang, J.-Y., and Lipscomb, W. N. (1991) *Proc. Natl. Acad. Sci. U. S. A.* **88,** 2989–2993
5. Marcus, F., Edelstein, I., Reardon, I., and Heinrikson, R. L. (1982) *Proc. Natl. Acad. Sci. U. S. A.* **79,** 7161–7165
6. Ke, H., Zhang, Y., Liang, J.-Y., and Lipscomb, W. N. (1990) *Proc. Natl. Acad. Sci. U. S. A.* **87,** 5243–5247
7. Zhang, Y., Liang, J.-Y, Huang, S., and Lipscomb, W. N. (1994) *J. Mol. Biol.* **244,** 609–624
8. Shyur, L. F., Aleshin, A. E., Honzatko, R. B., and Fromm, H. J. (1996) *J. Biol. Chem.* **271,** 33301–33307
9. Choe, J.-Y., Poland, B. W., Fromm, H. J., and Honzatko, R. B. (1998) *Biochemistry* **33,** 11441–11450
10. Choe, J.-Y., Fromm, H. J., and Honzatko, R. B. (2000) *Biochemistry* **39,** 8565–8574
11. Kurbanov, F. T., Choe, J.-Y., Honzatko, R. B., and Fromm, H. J. (1998) *J. Biol. Chem.* **273,** 17511–17516
12. Stone, S. R., and Fromm, H. J. (1980) *Biochemistry* **19,** 620–625
13. Nimmo, H. G., and Tipton, K. F. (1975) *Eur. J. Biochem.* **58,** 567–574
14. Lui, F., and Fromm, H. J. (1990) *J. Biol. Chem.* **265,** 7401–7406
15. Pilkis, S. J., El-Maghrabi, R. M., McGrane, M. M., Pilkis, J., and Claus, T. H. (1981) *J. Biol. Chem.* **256,** 3619–3622
16. Lui, F., and Fromm, H. J. (1988) *J. Biol. Chem.* **263,** 9122–9128
17. Shyur, L. F., Poland, B. W., Honzatko, R. B., and Fromm, H. J. (1997) *J. Biol. Chem.* **272,** 26295–26299
18. Carcamo, J. G., Yanez, A. J., Ludwig, H. C., Leon, O., Pinto, R. O., Reyes, A. M., and Slebe, J. C. (2000) *Eur. J. Biochem.* **267,** 2242–2251
19. Laemmli, U. K. (1970) *Nature* **227,** 680–685
20. Bradford, M. M. (1976) *Anal. Biochem.* **72,** 248–252
21. Leatherbarrow, R. J. (1987) *ENZFITTER: A Non-Linear Regression Data Analysis Program for the IBM PC*, pp. 13–75, Elsevier Science Publishers B. V., Amsterdam
22. Lakowicz, J. R. (1999) *Principles of Fluorescence Spectroscopy*, 2nd Ed., pp. 52–54, Kluwer Academic/Plenum Publishers, New York
23. Xue, Y., Huang, S., Liang, J.-Y, and Lipscomb, W. N. (1994) *Proc. Natl. Acad. Sci. U. S. A.* **91,** 12482–12486
24. Brünger, A. T. (1992) *XPLOR*, Version 3.1, Yale University Press, New Haven, CT
25. Nelson, S. W., Iancu, C. V., Choe, J.-Y., Honzatko, R. B., and Fromm, H. J. (2000) *Biochemistry*, in press
26. Horecker, B. L., Melloni, E., and Pontremoli, S. (1975) *Adv. Enzymol. Relat. Areas Mol. Biol.* **42,** 193–226
27. Scheffler, J. E., and Fromm, H. J. (1986) *Biochemistry* **25,** 6659–6665
28. Iverson, L. F., Brzozowski, M., Hastrup, S., Hubbard, R., Kastup, J. S., Larsen, I. K., Naerum, L., Norsko-Lauridsen, L., Rasmussen, P. B., Thim, L., Wiberg, F. C., and Lundgren, K. (1997) *Protein Sci.* **6,** 971–982
29. Shyur, L. F., Zhang, R., and Fromm, H. J. (1995) *J. Biol. Chem.* **270,** 123–127
30. Schaftingen, E. V., and Hers, H.-G. (1981) *Proc. Natl. Acad. Sci. U. S. A.* **78,** 2861–2863
31. Pilkis, S. J., El-Maghrabi, R. M., McGrane, M. M., Pilkis, J., and Claus, T. H. (1981) *J. Biol. Chem.* **256,** 11489–11495
32. Kraulis, J. (1991) *J. Appl. Crystallogr.* **24,** 946–950
33. Merritt, E. A., and Bacon, D. J. (1997) *Methods Enzymol.* **277,** 505–524

Mutations in the Hinge of a Dynamic Loop Broadly Influence Functional Properties of Fructose-1,6-bisphosphatase

Scott W. Nelson, Jun-Yong Choe, Richard B. Honzatko and Herbert J. Fromm

J. Biol. Chem. 2000, 275:29986-29992.
doi: 10.1074/jbc.M000473200 originally published online July 14, 2000
